A&A 494, 1013–1019 (2009)
DOI: 10.1051/0004-6361:200810219

Astronomy & Astrophysics

INTEGRAL and *XMM-Newton* observations of AX J1845.0−0433⋆

J. A. Zurita Heras[1] and R. Walter[2]

[1] Laboratoire AIM, CEA/DSM-CNRS-Université Paris Diderot, IRFU/Service d'Astrophysique, 91191 Gif-sur-Yvette, France
e-mail: juan-antonio.zurita-heras@cea.fr
[2] *INTEGRAL* Science Data Centre, Observatoire de Genève, Université de Genève, Chemin d'Ecogia 16, 1290 Versoix, Switzerland
e-mail: roland.walter@unige.ch

Received 19 May 2008 / Accepted 30 October 2008

ABSTRACT

Aims. AX J1845.0−0433 is a transient high-mass X-ray binary discovered by *ASCA*. The source displays bright and short flares observed by *INTEGRAL*. The transient behaviour and bright and short flares are studied to understand both the accretion mechanisms and nature of the source.
Methods. Public *INTEGRAL* data and a pointed *XMM-Newton* observation are used to study in detail the flaring and quiescent phases.
Results. AX J1845.0−0433 is a persistent X-ray binary with a O9.5I supergiant companion, emitting at a low 0.2−100 keV luminosity of $\sim 10^{35}$ erg s^{-1} with seldom flares and reaching luminosities of 10^{36} erg s^{-1}. The most accurately measured X-ray position is RA (2000) = $18^{\rm h}45^{\rm m}01.4^{\rm s}$ and Dec = −04°33′57.7″ (2″). Variability factors of 50 are observed on timescales as short as hundreds of seconds. The broad-band spectrum is typical of wind-fed accreting pulsars with an intrinsic absorption of $N_{\rm H} = (2.6 \pm 0.2) \times 10^{22}$ cm^{-2}, a hard continuum of $\Gamma = (0.7–0.9) \pm 0.1$, and a high-energy cutoff at $E_{\rm cut} = 16^{+5}_{-3}$ keV. An excess at low energies is also observed fitted with a black body with a temperature of $kT = 0.18 \pm 0.05$ keV. Optically-thin and highly-ionised iron (Fe XVIII−XIX) located close to the supergiant star is detected during the quiescence phase. The spectral shape of the X-ray continuum remains unchanged. In contrast to the persistent quiescent emission, the flare characteristics suggest that clumps of mass $M \sim 10^{22}$ g are formed within the stellar wind of the supergiant companion.

Key words. X-rays: binaries – X-rays: individuals: AX J1845.0−0433

1. Introduction

In classical supergiant HMXB (SGXB), the persistent X-ray emission is explained by accretion of part of the stellar wind of the supergiant star onto the compact object situated in a close circular orbit (see reviews by White et al. 1995; Psaltis 2006). The observed variability was explained in terms of wind instabilities generated by the interaction of the compact object with the strong stellar wind (Blondin et al. 1990; Blondin 1994). However, transient SGXB with intensity dynamic ranges of 10^{3-4} have been discovered (e.g. González-Riestra et al. 2004; Smith et al. 2006). These sources of low quiescent luminosities challenge the classical view of SGXB. These enormous flares are probably due to the clumpiness of the strong stellar wind (in't Zand 2005; Walter & Zurita Heras 2007; Negueruela et al. 2008), which is expected in OB supergiant stars (Oskinova et al. 2007, and references therein). The presence of a strong magnetic field can play an important role in the sharp, intensity transition (Bozzo et al. 2008).

AX J1845.0−0433 was discovered with *ASCA* while monitoring the Scutum Arm region on Oct. 18–24, 1993 (6 pointings of 20 ks each) (Yamauchi et al. 1995). The source was first detected at low intensity for several hours, and then entered into a flaring state in which the source average flux increased by a factor of 100 and exhibited several peaks each lasting tens of minutes. All detections are reported in Table 1. The flare spectrum was fitted with an absorbed, flat, power-law function with $\Gamma = 1.00 \pm 0.07$ and $N_{\rm H} = (3.6 \pm 0.3) \times 10^{22}$ cm^{-2}, typical of accreting pulsars (White et al. 1995). The X-ray spectrum showed no evolution. No coherent pulsation was observed with *ASCA* for periods between 125 ms and 4096 s. Coe et al. (1996) pinpointed the optical counterpart as being a O9.5I supergiant star located at RA (2000) = $18^{\rm h}45^{\rm m}01.5^{\rm s}$ and Dec = −04°33′55.5″ (unc. ∼1″) and estimated a distance to the source of ∼3.6 kpc. Since the source is a transient supergiant high-mass X-ray binary (HMXB), Negueruela et al. (2006) proposed that it is a supergiant fast X-ray transient (SFXT) candidate.

New detections of this transient were reported when Halpern & Gotthelf (2006) identified IGR J18450−0435 to be the hard X-ray counterpart of AX J1845.0−0433, after refining the *ASCA* position. Molkov et al. (2004) and Sguera et al. (2007) reported the average and flaring intensity activity of the source as observed with *INTEGRAL* and *Swift* (see Table 1). The flare duration was typically a few tens of minutes with sharp-rising/decaying times of a few minutes. The *Swift* X-ray spectra could be represented by similar absorbed, flat, power-law functions. Due to its recurrent, fast, X-ray flaring behaviour, they concur with its classification as a SFXT.

In this paper, we present results from a pointed *XMM-Newton* observation of AX J1845.0−0433 (P.I. Walter) and *INTEGRAL* archival data. We present the observations and describe the data reduction in Sect. 2. In Sect. 3, we present the results of revisions in X-ray astrometry and the temporal and

⋆ Based on observations with 1) *INTEGRAL*, an ESA project with instruments and science data centre funded by ESA member states (especially the P.I. countries: Denmark, France, Germany, Italy, Switzerland, Spain), Czech Republic and Poland, and with the participation of Russia and the USA and 2) *XMM-Newton*, an ESA science mission with instruments and contributions directly funded by ESA Member States and NASA.

Table 1. Summary of previous detections of AX J1845.0−0433.

Date UTC	Energy range keV	Flux 10^{-10} erg cm^{-2} s^{-1}
Oct. 19, 1993 13–21 h[1]	0.7–10	0.03
Oct. 19 22 h–20 05 h, 1993[1]	0.7–10	3
Mar.–May 2003[2]	18–60	0.2
Apr. 28, 2005[3]	20–40	4.5
Apr. 20, 2006[3]	20–40	6.0
Nov. 11, 2005[4]	0.2–10	1.1
Mar. 5, 2006[4]	0.2–10	2.3

[1] *ASCA*, Yamauchi et al. (1995).
[2] *INTEGRAL*, exposure 830 ks, Molkov et al. (2004).
[3] *INTEGRAL*, peak flux, Sguera et al. (2007).
[4] *Swift*, peak flux, Sguera et al. (2007).

spectral analysis. We discuss the temporal behaviour, accretion, and nature of the source in Sect. 4. Conclusions are summarised in Sect. 5.

2. Observations and data analysis

2.1. INTEGRAL

The INTErnational Gamma-Ray Astrophysics Laboratory (*INTEGRAL*) is a spacecraft that has operated since October 2002 on a 3-day, highly-eccentric orbit (Winkler et al. 2003). The scientific payload consists of four instruments. However, only data from the hard X-ray and soft γ-ray coded-mask imager IBIS/ISGRI (15−300 keV, field of view (FOV) of 29° square, angular resolution of 12′, Ubertini et al. 2003; Lebrun et al. 2003) will be considered in this work.

All public data available until Mar. 2007 (i.e. 2075 pointings with the source off-axis angle <14° and exposure >600 s) has been analysed. These pointings are distributed on 96 spacecraft revolutions between Mar. 19, 2003 (revolution 49, MJD 52 708.4) to Nov. 21, 2005 (revolution 379, MJD 53 695.5). The total exposure time of source is 4.8 Ms spanned over 2.5 years of observations. They were not equally distributed during this period because of scheduling reasons.

The ISGRI data are reduced using the Offline Scientific Analysis (OSA[1]) software version 6.0, which was publicly released by the *INTEGRAL* Science Data Centre (ISDC) (Courvoisier et al. 2003). Individual sky images for each pointing were produced in the energy band 22−50 keV with typical exposure time of ∼2−3 ks. The source count rate was extracted with the OSA tool `mosaic_spec` (version 1.4) for which the position was fixed to our *XMM-Newton* position and the point-spread function width was fixed to 6′. Detections were considered to be significant at a level of $\geq 5.1\sigma$. To search for the source quiescent level, we compiled deep-sky mosaics (of exposure times 50−1000 ks) disregarding all the pointings for which the source was detected. Detection of the source in deep mosaics is considered to be robust at a significance level of $\geq 6\sigma$. Two methods were used to extract the spectrum of the source. If the source was detected significantly in each individual pointing, the source spectra were extracted at each pointing with `ii_spectra_extract` and summed to create an average spectrum using `spe_pick`. Otherwise, the spectra were extracted from the deep-mosaic images with `mosaic_spec`. The redistribution matrix file (RMF) `isgr_rmf_grp_0023.fits` was rebinned into 5 channels spread between 15 and 80 keV, light curves with a binning of 10 s were extracted for each individual flares with `ii_light` version 8.2. The light curves were displayed in counts s^{-1}. The 22−50 keV count rates can be converted with the relation 1 Crab = 117 counts s^{-1} = 9×10^{-9} erg cm^{-2} s^{-1}.

[1] OSA is available at `http://isdc.unige.ch/?Soft+download`.

2.2. XMM-Newton

The main scientific instrument onboard the X-ray Multi-Mirror Mission (*XMM-Newton*, Jansen et al. 2001) satellite is the EPIC camera consisting of two MOS (Turner et al. 2001) and one pn (Strüder et al. 2001) CCD cameras. It has imaging, timing, and spectral capabilities in the 0.2−12 keV energy range with a 30′ FOV. The EPIC cameras operated in imaging science mode with full window and medium filters.

AX J1845.0−0433 was observed with *XMM-Newton* on April 3, 2006, from 15:01:33 to 20:21:46 UTC (MJD 53 828.627−53 828.849) for a total exposure time of 19 ks. There was no simultaneous observation with *INTEGRAL*.

Event lists for each of the MOS and pn cameras were generated by the Science Analysis Software (SAS[2]) version 7.0.0 using the `emproc` and `epproc` tool, respectively. The observation was not affected by enhanced background features, and all events were detected in images for a total exposure time of 19 ks for both MOS and 17 ks for pn. Images for MOS[12] and pn were generated at 2″ and 4″ resolution, respectively, using good events up to the quadruple level in the 0.8−10 keV energy range and disregarding bad pixels. An accurate X-ray position was determined by using EPIC and the SAS task `edetect_chain`. Four images with energy ranges of 0.5−2, 2−4.5, 4.5−7.5, and 7.5−12 keV for each of the MOS and pn cameras were extracted. The most accurate position for each individual EPIC camera was then determined. Finally, the most reliable source position was calculated to be the mean of the positions given by the three cameras. The source location accuracy was limited by the spacecraft astrometry of 2″[3], the statistical error of 0.04″ being insignificant in comparison.

In the EPIC/pn image, the event list of the source+background was extracted from a region of 30″ radius centred on the source. A background event list was extracted in the same CCD at the same distance as the read-out node from a region of similar size unaffected by the bright source. Spectra extracted by identifying only single events but disregarding bad pixels. Specific RMF and ancillary response files (ARF) were generated with the SAS tasks `rmfgen` and `arfgen`, respectively. The `Xspec` version 11.3.2t package (Arnaud 1996) was used to plot and fit the final spectra, which had been corrected from background. For light curves, single and double events were selected. The source light curve was corrected for the background signal by using the SAS task `lccorr`. We applied the barycentric correction with the SAS task `barycen`.

3. Results

3.1. Refined X-ray position

A 22–50 keV ISGRI image was generated from pointings in which the source was detected (see Fig. 2). The source was

[2] SAS is available at `http://xmm.vilspa.esa.es/external/xmm_sw_cal/sas.shtml`.
[3] The *XMM-Newton* astrometric accuracy is described in the calibration document `XMM-CAL-TN-0018`.

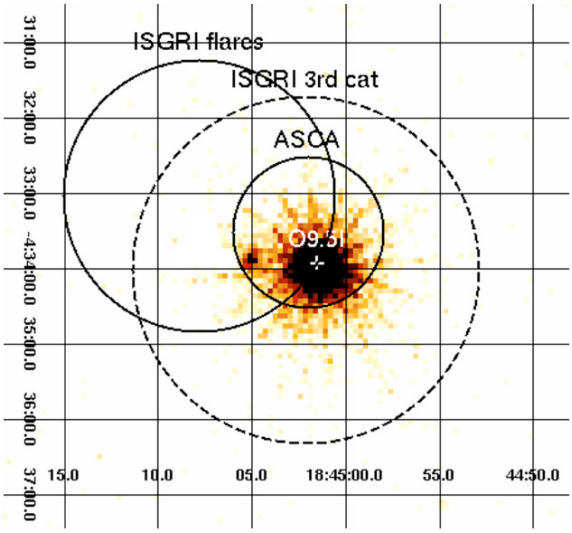

Fig. 1. EPIC/MOS1 image in the 0.8−10 keV energy range. The optical counterpart of AX J1845.0−0433 is indicated by a cross labelled with its spectral type. Its position coincides with that of the X-ray source. Only the ISGRI (derived from the flares and from the 3rd ISGRI catalogue) and the ASCA error boxes are reported for easier visibility. The *Swift* position is well embedded in the *XMM-Newton* source.

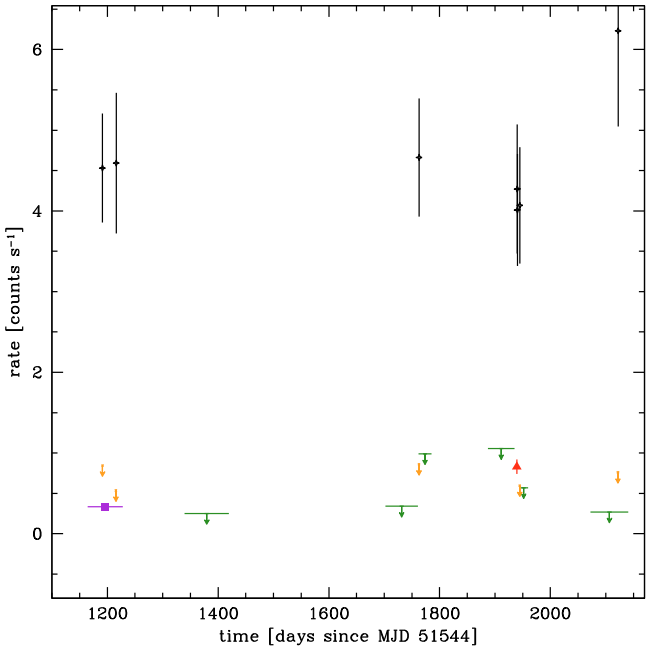

Fig. 2. ISGRI 22−50 keV long-term light curve of AX J1845.0−0433. Detections in single pointings with exposure times of ∼2 ks are shown with crosses and error bars. Disregarding the flares, the triangle corresponds to the average source flux during revolution 308. The box corresponds to a detection in the first deep mosaic with an exposure time of 1.2 Ms. Otherwise, 5σ upper limits are represented (with exposure times of $\sim 10^{2-3}$ ks).

detected at a confidence level of 17σ for a total exposure time of 17.3 ks. The most robust hard X-ray position was RA (2000) = $18^h45^m07.8^s$ and Dec = $-04°33'01.2''$ with an error of 1.8′ (Gros et al. 2003). This position was consistent with the position given in the 3rd ISGRI catalogue (Bird et al. 2007).

One bright source corresponds to the AX J1845.0−0433 position in EPIC images (see Fig. 1). The most reliable position determined with EPIC was RA (2000) = $18^h45^m01.4^s$ and Dec = $-04°33'57.7''$ with an uncertainty of 2″. It is located 2.9″ away from the optical counterpart given by Coe et al. (1996). This X-ray revised position is consistent with the position of the counterpart to within the respective error boxes. It is also consistent with the *ASCA* and *INTEGRAL* positions. The *Swift* position is outside the EPIC error box (8″ away), although no *Swift* positional uncertainty was given by Sguera et al. (2007).

3.2. Timing analysis

We first explored the long-term behaviour of the source with *INTEGRAL*, and then, we focused on the short-term variability using *XMM-Newton*.

3.2.1. Long-term variability

The 22−50 keV long-term variability of AX J1845.0−0433 is shown in Fig. 2. The source was detected in only 7 pointings out of 2075 with average (over the pointing duration) count rates of within 4−6 cts s^{-1} (=34−51 mCrab) (cross points in Fig. 2). These rare detections in single pointings are considered to be flares. They are randomly distributed among the 2.5 yr observations. Two detections were separated by 4 h. This could be indicative of a longer flare because the source was at the limit of detectability (see Table 2). We constructed mosaics for each of the 96 revolutions, discarding the 7 pointings reported above. The source was detected only in revolution 308: exposure 159 ks, significance 9σ, and count rate 0.83 ± 0.09 cts s^{-1} (=7.1 ± 0.8 mCrab) (triangle in Fig. 2). To avoid contamination close to the flares, we also tested the presence of the source by discarding the final part of the revolution stopping 20 ks before the flares. For an exposure time of 134 ks, the source was still detected at a 7.4σ significance level for a count rate of 0.7 ± 0.1 cts s^{-1}. The source varied in intensity by a factor of 5 between the flares and the low-level emission during revolution 308. For the other 5 revolutions in which at least one flare occurred (i.e. 58, 66, 249, 310 and 369), the source was not detected with a 5σ significance level upper limit in the range 0.5−1.0 cts s^{-1} (=4.5–8.5 mCrab), which is represented by cross-arrows in Fig. 2. During rev. 308, there was evidence of a long period of activity, but no evidence for such behaviour in the other revolutions where only one isolated flare was detected.

Data from revolutions that had no detection were accumulated together in units of 30 days. The source was only detected in the first deep mosaic of 1.2 Ms at a confidence level of 9σ with a count rate of 0.33 ± 0.04 cts s^{-1} (=2.8 ± 0.3 mCrab) (box in Fig. 2). For the other 6 mosaics, the 5σ upper limit level was in the range 0.2−1.0 cts s^{-1} (=0.25−8.5 mCrab).

Data from the 6 deep mosaics with non-detection were accumulated to construct a very-deep mosaic. The source was

Table 2. List of flares of AX J1845.0−0433 observed with *INTEGRAL*/IBIS/ISGRI.

Time MJD−51 544	22–50 keV flux cts s^{-1}	On-time exp. ks	Pointing
1191.2173	4.5 ± 0.7	2.2	00580043
1216.0800	4.6 ± 0.9	1.8	00660092
1763.0657	4.7 ± 0.7	3.0	02490072
1940.2455	4.3 ± 0.8	2.0	03080097
1940.4107	4.0 ± 0.7	3.5	03080103
1944.8607	4.1 ± 0.7	2.0	03100044
2122.4849	6.2 ± 1.2	3.0	03690058

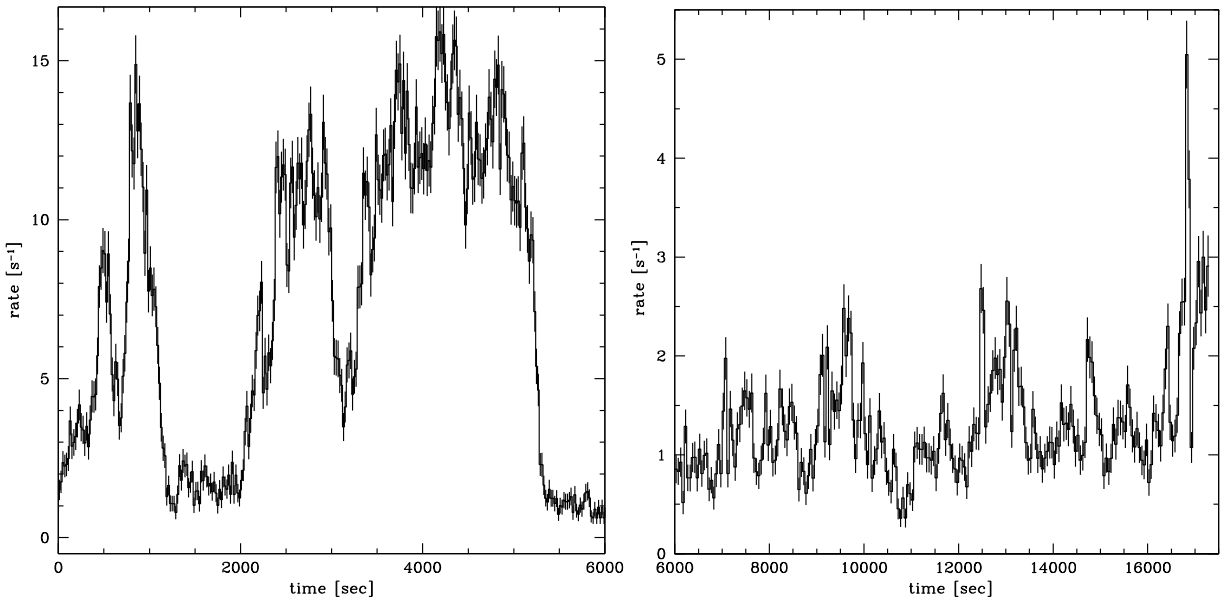

(a) Flare state (bin=20 s). (b) Quiescent state (bin=50 s).

Fig. 3. EPIC/pn 0.4−10 keV light curve of AX J1845.0−0433 divided into two parts to show the flare (*left*) and quiescent (*right*) state (T0 = MJD 53 828.6430).

detected at a confidence level of 9.2σ with 0.25 ± 0.03 cts s^{-1} (=2.1 ± 0.3 mCrab) for an exposure time of 2.6 Ms. This corresponds to a factor of 25 lower in intensity than the brightest flare detected in pointing `03690058`. We conclude that the quiescent level is ∼2.5 mCrab.

3.2.2. Short-term variability

The EPIC/pn 0.4−10 keV light curve is displayed in Fig. 3. During the first 5 ks, AX J1845.0−0433 exhibited two short and complex flares lasting 1 ks and 3 ks, respectively. Both flares behaved similarly with sharp rises/decays in intensity that varied between ∼2−12 cts s^{-1} on timescales of a few hundred of seconds. During the flares, variations were also significant with short peaks reaching ∼15 cts s^{-1} (maximum 16.2 ± 0.6 cts s^{-1}). Abrupt and short ($\lesssim$300 s) decays in intensity of as low as ∼4 cts s^{-1} also occurred within the flares, although the quiescent level was not reached. The flare durations were comparable with those observed by *INTEGRAL*.

After the two flares, the source intensity remained at a low level (average count rate of 1.2±0.2 cts s^{-1}) and showed continuous variability of a factor of 2−3 with several peaks of >2 cts s^{-1} (see Fig. 3(b)). Taking into account the entire observation, the variability factor between the lowest and highest 0.4−10 keV count rate was 45. Towards the end of the observation, there was a flare-like event lasting only ∼50 s that reached an intensity of 5.2 ± 0.3 cts s^{-1}.

We also searched for pulsations during the time interval of 0.1−5000 s in the EPIC/pn light curve, although a pulsation was observed neither during the flare nor during the quiescence phase.

3.3. Spectral analysis

The source exhibited two emission states in the X-rays: a quiescence emission randomly interrupted by rare sharp and short flares. Therefore, one X-ray spectrum was extracted for each of the states. Spectrum events lists were selected from good time intervals created from the 0.4–10 keV light curve using the criteria that the rate was ≥6 cts s^{-1} for the flare and ≤3 cts s^{-1} for the quiescent spectra, respectively. The spectral bins were grouped to have at least 100 counts and 50 counts per channel for the flare and quiescent spectra, respectively. Therefore, the χ^2 statistic was used throughout the spectral analysis (χ^2_ν is used to denote the reduced χ^2). Concerning the hard X-rays, the flare spectrum was extracted by combining the seven detections. The quiescent spectrum was extracted from the deep mosaic image, which represented the 9σ detection.

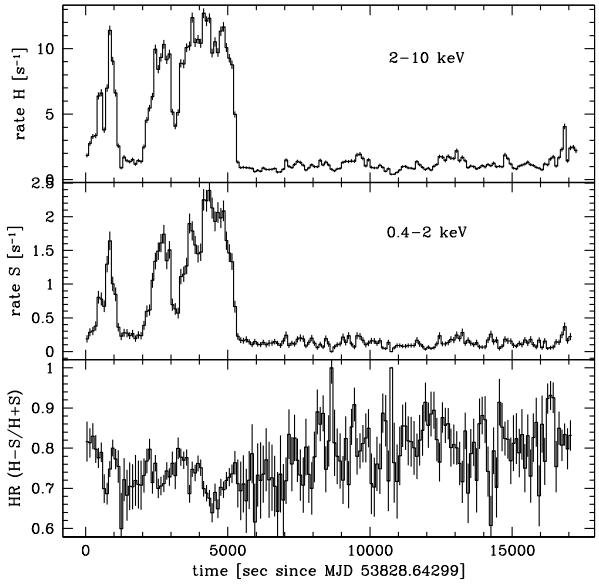

Fig. 4. EPIC/pn hardness ratio light curve of AX J1845.0−0433 (bin 100 s).

To search for spectral variations, the hardness ratio (HR ≡ $(H-S)/(H+S)$) was calculated from two light curves for the energy ranges of $S \equiv 0.4$−2 keV and $H \equiv 2$−10 keV (see Fig. 4). The HR varies between the flare and the quiescence phases

with $\langle HR_{flare} \rangle = 0.717 \pm 0.005$ and $\langle HR_{quiesc} \rangle = 0.795 \pm 0.007$, indicating a slight softening of the spectrum during the flare.

EPIC/pn and ISGRI spectra were fitted together using a multiplicative constant (C_{ISGRI}) to take account of the cross-calibration between instruments. The constant was fixed to 1 for EPIC/pn and remained free for ISGRI. Photoelectric absorption was included in all models. A power-law (PL) or a black body (BB) function clearly failed to reproduce the flare spectrum with χ^2_ν of 1.76 and 1.94 (both 207 d.o.f.), respectively. An energy break was required at high-energies. Therefore, a broken PL and a PL with a high-energy cutoff were used (in Xspec, `bknpower` and `cutoffpl`, respectively, thereafter BKN and CPL). The χ^2_ν were improved to 1.49 (205 d.o.f.) and 1.18 (206 d.o.f.), respectively. A slight excess was observed at low energies (<2 keV). The addition of a BB function at low temperature $kT \sim 0.1$ keV improved the χ^2_ν statistical fit down to 0.95 (204 d.o.f.).

For the quiescent spectrum, absorbed PL or BB models were unable to reproduce the data for a reasonable cross-calibration constant. We therefore applied the BKN and CPL models. The CPL model again provided the closest fit with a χ^2_ν of 1.43 (125 d.o.f.). A sharp decline in the spectrum data is clearly visible at energies higher than 8 keV in the EPIC/pn part compared with the model. An edge multiplicative component was added to the model, improving the χ^2_ν to 1.17 (121 d.o.f.). A soft excess at energies lower than 2 keV was also observed in the quiescent spectrum, and we therefore also added a soft BB ($kT \sim 0.1$ keV). This resulted in a final χ^2_ν of 1.00 (121 d.o.f.).

The soft component observed in both quiescent and flaring spectra can also be modelled as emission from an optically-thin plasma (`mekal`, Kaastra 1992, and references therein). The results were almost identical for the `bb` and `mekal` models with similar $\chi^2_\nu \sim 0.9$ (324 d.o.f.).

The source spectrum consisted of two components with a thermal component dominating at low energies ($\lesssim$2 keV) and a hard power-law continuum with a high-energy cutoff (>10 keV), to which an inter-calibration constant, absorption, and an edge were added[4]. The parameters were allowed to vary freely between flare and quiescent spectra, apart from the edge energy that was fixed to the value found in the quiescent spectrum, and the high-energy cutoff was fixed to the value found in the flaring state. The column density and temperature of the soft component did not differ significantly between the flare and quiescent spectra. Therefore, these parameters were fitted simultaneously:

- the parameters in fitting both spectra: $N_H = (2.6 \pm 0.2) \times 10^{22}$ cm^{-2}, $E_{edge} = 7.9 \pm 0.1$ keV, $kT = 0.18 \pm 0.05$ keV and $E_{cut} = 16^{+5}_{-3}$ keV;
- flare spectrum: $N_{mekal} = 0.8^{+5.7}_{-0.6}$ cm^{-5}, $\tau_{edge} = 0.19 \pm 0.08$, $\Gamma = 0.9 \pm 0.1$, $C_{ISGRI} = 2.3^{+0.7}_{-0.5}$ and the unabsorbed fluxes are 1.2×10^{-9} erg cm^{-2} s^{-1} (0.4–10 keV) and 2.9×10^{-10} erg cm^{-2} s^{-1} (20–100 keV); and
- quiescent spectrum: $N_{mekal} = 0.06^{+0.32}_{-0.05}$ cm^{-5}, $\tau_{edge} = 0.5 \pm 0.1$, $\Gamma = 0.7 \pm 0.1$, $C_{ISGRI} = 0.9^{+0.4}_{-0.3}$ and the unabsorbed fluxes are 0.9×10^{-10} erg cm^{-2} s^{-1} (0.4–10 keV) and 1.7×10^{-11} erg cm^{-2} s^{-1} (20–100 keV),

with $\chi^2_\nu \sim 0.9$ (326 d.o.f.) (see Fig. 5).

4. Discussion

Our *XMM-Newton* astrometry has confirmed the supergiant counterpart of AX J1845.0−0433 reported by Coe et al. (1996).

[4] The Xsepc model is: `cons*wabs*edge*(mekal+cutoffpl)`.

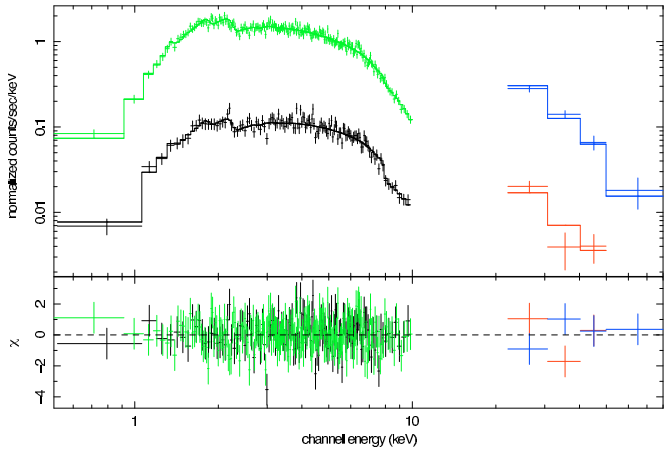

Fig. 5. Broad-band spectra of AX J1845.0−0433. The flare and quiescent spectra are displayed in *the top panel*. The spectra were fitted simultaneously with the following model: `cons*wabs*edge*(mekal+cutoffpl)`. Residuals are shown in *the bottom panel*.

4.1. Persistence of the source

At a distance of 3.6 kpc, the quiescent average 0.4–10 and 20–100 keV luminosities of AX J1845.0−0433 are 1.4×10^{35} erg s^{-1} and 2.7×10^{34} erg s^{-1}, respectively. During the flares, the average 0.4–10 and 20–50 keV luminosities were 1.8×10^{36} erg s^{-1} and 4.5×10^{35} erg s^{-1}, respectively. During the quiescence phase, the source exhibited continuous variability (of a factor of 2, see Fig. 3). Discarding these mini-flares, the minimum source 0.4–10 keV luminosity became as low as 1.1×10^{34} erg s^{-1}. The emission observed by *Swift*/XRT (see Figs. 4 and 5 in Sguera et al. 2007) was also consistent with the quiescent emission observed by EPIC. This quiescent emission was also observed with *ASCA* (although the data were of low quality). This persistent and variable emission indicated that the source must be accreting permanently because this luminosity was too high to be explained by the X-ray luminosity of 10^{30-33} erg s^{-1} detected in single OB stars (Berghoefer et al. 1997, and references therein).

We consider a compact object of mass $M_X = 1.4\ M_\odot$ and radius $R_X = 10$ km. For a O9.5I supergiant star, the most probable stellar parameters are $M_* \sim 30\ M_\odot$, $R_* \sim 23\ R_\odot \sim 1.6 \times 10^{12}$ cm, $\log(L_*/L_\odot) \sim 5.5$, and $T \sim 3 \times 10^4$ K (Martins et al. 2005). The average parameters of the stellar wind for a O9.5I massive star are a terminal velocity of $v_\infty = 1765$ km s^{-1} (Prinja et al. 1990) and an escape velocity of $v_\infty/v_{esc} = 2.6$ (Lamers et al. 1995). These values imply a theoretical stellar mass-loss rate of $\dot{M}_{wind} \sim 9.4 \times 10^{-7}\ M_\odot$ yr^{-1} (see Eq. (12) of Vink et al. 2000). The average mass-accretion rate can be estimated to be $\dot{M}_{accr} = L_X/\epsilon c^2 = 3.5 \times 10^{-11}\ M_\odot$ yr^{-1}, where $\epsilon = 0.1$ is the accretion efficiency and c the speed of light. The accretion radius is $R_{accr} = 2GM_X/(v^2_{wind} + v^2_X)$, where the stellar wind velocity is $v_{wind} = v_\infty(1 - R_*/r)^\beta$ with $\beta \approx 1$ (Kudritzki & Puls 2000, and reference therein) and v_X is the compact-object velocity. We can relate $\dot{M}_{accr}$ to $\dot{M}_{wind}$ with $\dot{M}_{accr} = (R^2_{accr}/4a^2)\,\dot{M}_{wind}$, where a is the binary separation. To explain a persistent quiescent luminosity of $\lesssim 2 \times 10^{35}$ erg s^{-1} in AX J1845.0−0433, one requires a binary separation of $a \gtrsim 5 \times 10^{12}$ cm $\sim 3\ R_*$, which is slightly higher than in classical SGXB ($a \approx 2\ R_*$).

The source experienced short episodes of highly-enhanced emission with flares reaching levels of a few 10^{36} erg s^{-1}, as observed by *ASCA*, *INTEGRAL*, and *XMM-Newton*. Only *Swift*

observations were unable to detect any strong flare of the source with a short exposure time. *INTEGRAL* detected 6 flares in 4.8 Ms of effective exposure, that is one flare on average every 9.2 days. This value can be considered to represent an upper limit because the average flare peak luminosity is just above the ISGRI sensitivity threshold when the source is within 9° from the FOV centre. For a larger angular angle, fluxes of 4−5 cts s^{-1} are below the 5σ significance level (considering a pointing timescale). Since in half of the pointings (53%), the source was farther than 9° from the FOV centre, the bright flare frequency could be estimated as being one flare every 4−5 days.

4.2. Source spectra

The spectra are fitted with models typically used for wind-fed accreting HMXB. The source is observed in two states of luminosity, the quiescence phase and the flaring phase. We note that the *INTEGRAL* and *XMM-Newton* observations are not simultaneous, explaining the high inter-calibration constant needed to reproduce the flare spectrum. For the quiescent spectrum that combines the average hard X-ray spectrum with an instantaneous X-ray spectrum, the inter-calibration constant is almost one. That implies that the accretion rate during the quiescent phase is almost constant. Therefore, the compact object would occupy a near-circular orbit, and the stellar wind, most of the time, would be rather homogeneous ($\Delta\rho/\rho \sim 2$).

The continuum was reproduced with a flat power-law ($\Gamma \sim 0.7 - 0.9$) and a high-energy cutoff of $E_{\rm cut} \sim 16$ keV. The absorbing column density of $N_{\rm H} = (2.6 \pm 0.2) \times 10^{22}$ cm^{-2} was higher than the entire interstellar absorption[5] expected along the line of sight $N_{\rm H} \sim 1.58 \times 10^{22}$ cm^{-2} (Dickey & Lockman 1990). The observed additional absorption corresponds to the expected local absorption estimated as $N_{\rm H} \approx \dot{M}_{\rm wind}/(8\ \mu m_{\rm H} v_{\rm wind} a) \sim 2.4 \times 10^{22}$ cm^{-2} for a NS orbiting in a circular orbit at $a = 3\ R_*$ around a massive star with a spherically symmetric stellar wind. When comparing the different observations of *ASCA*, *Swift*, and *XMM-Newton*, the column density varied slightly by a factor of 2 at maximum between $(1.6–3.6) \times 10^{22}$ cm^{-2}, while the power-law Γ remained comparable in each case. Variation in the column density has been observed in other SGXB (e.g. Haberl et al. 1989; Prat et al. 2008) and explained by the interaction between the stellar wind and X-ray emission of the compact object (Blondin et al. 1990, 1991). For the few HMXB that have been monitored, these variations are of higher factors such as 10. However, for AX J1845.0−0433 only 4 measurements of $N_{\rm H}$ presently exist, and the orbital period of the system is unknown.

A soft excess is also observed at low energies and reproduced with an optically-thin plasma of temperature $kT = 0.18 \pm 0.05$ keV. Assuming $n_{\rm e} \sim n_{\rm H} \sim \dot{M}_{\rm wind}(a)/(4\pi a^2 \mu m_{\rm H} v_{\rm wind}(a)) \sim 10^9$ cm^{-3} for $a \gtrsim 3\ R_*$, the size of the soft X-ray emitting region (sphere of radius $R_{\rm em}$) can be estimated from the mekal normalisation to be $R_{\rm em} \approx \sqrt[3]{3\, N_{\rm mekal}/10^{-14} \times (D_{\rm a}/n_{\rm H})^2}$, which corresponds to $R_{\rm em}^{\rm quies} \sim 10^{13}$ cm $\sim 8\ R_*$ and $R_{\rm em}^{\rm flare} \sim 3 \times 10^{13}$ cm $\sim 20\ R_*$. Therefore, the soft X-ray excess is emitted within the stellar wind. Such excess has been observed in other HMXB and appears to be a common feature of these systems (Hickox et al. 2004). They are probably due to X-ray scattering or partial ionization in the stellar wind (White et al. 1995).

The second distinctive feature observed in the spectrum, especially in the quiescent one, is the absorption edge present at 7.9 keV. In other HMXB such as 4U 1700−37 (van der Meer et al. 2005) or Vela X−1 (Nagase et al. 1986), absorption edges related to the K-edge absorption threshold of near-neutral iron have been observed at energies $E_{\rm edge} \gtrsim 7.1$ keV. However, the edge energy detected in AX J1845.0−0433 is significantly higher and would correspond to highly-ionized iron of level XVIII and XIX (see Fig. 7 of Nagase et al. 1986) or (Fig. 2 of Kallman et al. 2004). The ionization parameter defined to be $\xi = L_{\rm X}/nr_{\rm X}^2$, where $L_{\rm X}$ is the X-ray luminosity of the source, n the gas density, and $r_{\rm X}$ the distance from the X-ray source characterizes the photoionization of the gas (Tarter et al. 1969). For Fe XVIII and XIX, the limits of ξ are $1 < \log(\xi) < 3$ (see Fig. 5 of Kallman et al. 2004). Since $\tau = n\sigma_{\rm Fe} r_{\rm X}$ where $\sigma_{\rm Fe}$ is the iron cross-section (that is $\sim 10^{-20}$−10^{-19} cm^2 for Fe XVIII and XIX at 7.9 keV; Kallman et al. 2004), the highly-ionized iron must be located at a distance of within $1.5 < \log(L_{\rm X}\sigma_{\rm Fe}/\tau r_{\rm X}) < 2.5$, so that $(6–63) \times 10^{12}$ cm $\sim 4–40\ R_*$, which is larger than $\gtrsim a$, the expected binary separation derived above. Thus, the highly-ionized iron is not located close to the compact object but is spread throughout the binary system.

4.3. Flares by clumpy winds

Most persistent SGXB exhibit luminosities of approximately of 10^{36} erg s^{-1} with frequent flares implying variation factors of the order of $\lesssim$20. For AX J1845.0−0433, we observe a persistent emission one order of magnitude lower than usual, and occasional strong flares exhibiting variation factors of $\gtrsim$20. The accretion radius $R_{\rm accr}$ defined above also implies a free-fall time of $t_{\rm ff} = 0.5(\pi R^{3/2}/\sqrt{2GM}) \sim 230$ s for matter accreted onto the compact object from $R_{\rm accr} \sim 2 \times 10^{10}$ cm. Since the increase/decrease time of flares observed in AX J1845.0−0433 ($t_{\rm incr/decr} = 100–850$ s) are also of this order, the infall matter producing the flares is radially accreted onto the compact object.

Walter & Zurita Heras (2007) demonstrated that the flaring emission from transient SGXB, the so-called SFXT, must occur by accretion of clumpy winds onto a NS orbiting at a larger distance than usual ($\sim 10\ R_{\rm star}$), displaying low quiescent emission (if observed) of $\lesssim 10^{33}$ erg s^{-1}, that imply variability factors of $\gtrsim$100 (see also Negueruela et al. 2008).

In quiescence, AX J1845.0−0433 is more luminous than typical SFXT. It also exhibits significant variability of factors of 2−3 as observed in other SGXB. The source has a behaviour that is in-between that of SFXT and SGXB. A clump/inter-clump density ratio of 45 is observed for AX J1845.0−0433. Thus, the inferred $\dot{M}$ is lower than usual, producing a persistent quiescent emission that is lower than in other SGXB but higher than in SFXT. The characteristics of the flares (number, luminosity, duration, increase/decrease time) observed in AX J1845.0−0433 imply that the source has accreted some of these clumps ($M \sim 10^{21–22}$ g), as described by Walter & Zurita Heras (2007).

5. Conclusion

AX J1845.0−0433 is most likely to be a persistent X-ray binary with a O9.5I supergiant companion that emits with a low 0.2−100 keV luminosity of $\sim 10^{35}$ erg s^{-1} with seldom flares reaching luminosities of 10^{36} erg s^{-1}. The most accurate X-ray position is RA (2000) = $18^{\rm h}45^{\rm m}01.4^{\rm s}$ and Dec = −04°33′57.7″ (2″). Variability factors of as high as 50 are observed on extremely short timescales (few ks). The broad-band spectrum is typical of wind-fed accreting pulsars with a slight

[5] The column density derived from the optical absorption $A_{\rm V} \sim 7.6$ (Coe et al. 1996) is $N_{\rm H} \sim 1.4 \times 10^{22}$ cm^{-2} using the relation derived by Predehl & Schmitt (1995).

intrinsic absorption of $N_{\rm H} = (2.6 \pm 0.2) \times 10^{22}$ cm^{-2}, a hard continuum of $\Gamma = (0.7{-}0.9) \pm 0.1$, and a high-energy cut-off at $E_{\rm cut} = 16^{+5}_{-3}$ keV. An excess at low energies is also observed when the data are fitted with a BB of temperature $kT = 0.18 \pm 0.05$ keV. The presence of optically-thin and highly-ionised iron (Fe XVIII−XIX) located far from the compact object but close to the companion star ($\gtrsim 4\,R_*$) is also observed, principally during the quiescence phase of the source. No spectral variations were detected between the flare and quiescence phases, apart from the luminosity and absorption depth of the 7.9 keV edge. The flare characteristics (number, luminosity, duration, increase/decrease time), in contrast to the persistent, quiescent emission, suggest that clumps of mass $M \sim 10^{22}$ g are formed within the stellar wind of the supergiant companion.

Acknowledgements. The authors thank the anonymous referee his useful comments that improved the manuscript. The authors acknowledge the use of NASA's Astrophysics Data System. J.A.Z.H. thanks J. Rodriguez and S. Chaty for giving useful comments.

References

Arnaud, K. A. 1996, in Astronomical Data Analysis Software and Systems V, ed. G. H. Jacoby, & J. Barnes, ASP Conf. Ser., 101, 17
Berghoefer, T. W., Schmitt, J. H. M. M., Danner, R., & Cassinelli, J. P. 1997, A&A, 322, 167
Bird, A. J., Malizia, A., Bazzano, A., et al. 2007, ApJS, 170, 175
Blondin, J. M. 1994, ApJ, 435, 756
Blondin, J. M., Kallman, T. R., Fryxell, B. A., & Taam, R. E. 1990, ApJ, 356, 591
Blondin, J. M., Stevens, I. R., & Kallman, T. R. 1991, ApJ, 371, 684
Bozzo, E., Falanga, M., & Stella, L. 2008, ApJ, 683, 1031
Coe, M. J., Fabregat, J., Negueruela, I., Roche, P., & Steele, I. A. 1996, MNRAS, 281, 333
Courvoisier, T. J.-L., Walter, R., Beckmann, V., et al. 2003, A&A, 411, L53
Dickey, J. M., & Lockman, F. J. 1990, ARA&A, 28, 215
González-Riestra, R., Oosterbroek, T., Kuulkers, E., Orr, A., & Parmar, A. N. 2004, A&A, 420, 589
Gros, A., Goldwurm, A., Cadolle-Bel, M., et al. 2003, A&A, 411, L179
Haberl, F., White, N. E., & Kallman, T. R. 1989, ApJ, 343, 409
Halpern, J. P., & Gotthelf, E. V. 2006, The Astronomer's Telegram, 692, 1
Hickox, R. C., Narayan, R., & Kallman, T. R. 2004, ApJ, 614, 881
in't Zand, J. J. M. 2005, A&A, 441, L1
Jansen, F., Lumb, D., Altieri, B., et al. 2001, A&A, 365, L1
Kaastra, J. S. 1992, Internal SRON-Leiden Report
Kallman, T. R., Palmeri, P., Bautista, M. A., Mendoza, C., & Krolik, J. H. 2004, ApJS, 155, 675
Kudritzki, R.-P., & Puls, J. 2000, ARA&A, 38, 613
Lamers, H. J. G. L. M., Snow, T. P., & Lindholm, D. M. 1995, ApJ, 455, 269
Lebrun, F., Leray, J. P., Lavocat, P., et al. 2003, A&A, 411, L141
Martins, F., Schaerer, D., & Hillier, D. J. 2005, A&A, 436, 1049
Molkov, S. V., Cherepashchuk, A. M., Lutovinov, A. A., et al. 2004, Astron. Lett., 30, 534
Nagase, F., Hayakawa, S., Sato, N., Masai, K., & Inoue, H. 1986, PASJ, 38, 547
Negueruela, I., Smith, D. M., Reig, P., Chaty, S., & Torrejón, J. M. 2006, in ESA SP-604: The X-ray Universe 2005, ed. A. Wilson, 165
Negueruela, I., Torrejón, J. M., Reig, P., Ribó, M., & Smith, D. M. 2008, Am. Inst. Phys. Conf. Ser., 1010, 252
Oskinova, L. M., Hamann, W.-R., & Feldmeier, A. 2007, A&A, 476, 1331
Prat, L., Rodriguez, J., Hannikainen, D. C., & Shaw, S. E. 2008, MNRAS, 389, 301
Predehl, P., & Schmitt, J. H. M. M. 1995, A&A, 293, 889
Prinja, R. K., Barlow, M. J., & Howarth, I. D. 1990, ApJ, 361, 607
Psaltis, D. 2006, Accreting neutron stars and black holes: a decade of discoveries (Compact stellar X-ray sources), 1
Sguera, V., Bird, A. J., Dean, A. J., et al. 2007, A&A, 462, 695
Smith, D. M., Heindl, W. A., Markwardt, C. B., et al. 2006, ApJ, 638, 974
Strüder, L., Briel, U., Dennerl, K., et al. 2001, A&A, 365, L18
Tarter, C. B., Tucker, W. H., & Salpeter, E. E. 1969, ApJ, 156, 943
Turner, M. J. L., Abbey, A., Arnaud, M., et al. 2001, A&A, 365, L27
Ubertini, P., Lebrun, F., Di Cocco, G., et al. 2003, A&A, 411, L131
van der Meer, A., Kaper, L., di Salvo, T., et al. 2005, A&A, 432, 999
Vink, J. S., de Koter, A., & Lamers, H. J. G. L. M. 2000, A&A, 362, 295
Walter, R., & Zurita Heras, J. 2007, A&A, 476, 335
White, N. E., Nagase, F., & Parmar, A. N. 1995, X-ray binaries, Cambridge Astrophysics Series, ed. W. H. G. Lewin, J. Van Paradijs, & E. P. J. Van den Heuvel (Cambridge, MA: Cambridge University Press), 1
Winkler, C., Courvoisier, T. J.-L., Di Cocco, G., et al. 2003, A&A, 411, L1
Yamauchi, S., Aoki, T., Hayashida, K., et al. 1995, PASJ, 47, 189